C. R. Acad. Sci. Paris, Ser. I 348 (2010) 105–110

Contents lists available at ScienceDirect

C. R. Acad. Sci. Paris, Ser. I

www.sciencedirect.com

Numerical Analysis

High-order dimensionally split Lagrange-remap schemes for compressible hydrodynamics

Schémas directions alternées d'ordre élevé de type Lagrange-projection pour l'hydrodynamique compressible

Frédéric Duboc, Cédric Enaux, Stéphane Jaouen, Hervé Jourdren, Marc Wolff

CEA, DAM, DIF, 91297 Arpajon, France

ARTICLE INFO

Article history:
Received 20 April 2009
Accepted after revision 9 December 2009
Available online 30 December 2009

Presented by Olivier Pironneau

ABSTRACT

We first propose a new class of finite volume schemes for solving the 1D Euler equations. Applicable to arbitrary equations of state, these schemes are based on a Lagrange-remap approach and are high-order accurate in both space and time in the nonlinear regime. A multidimensional extension on *nD* Cartesian grids is then proposed, using a high-order dimensional splitting technique. Numerical results up to 6th-order are provided.

RÉSUMÉ

Nous proposons une nouvelle souche de schémas volumes finis pour résoudre les équations d'Euler 1D. Ces schémas, basés sur le formalisme Lagrange-projection, sont d'ordre élevé en régime non linéaire et en formulation équation d'état arbitraire. Une extension multi-dimensionnelle par splitting directionnel d'ordre élevé sur grille cartésienne est alors proposée, illustrée de résultats numériques jusqu'à l'ordre 6.

Version française abrégée

De nombreuses souches de schémas de grande précision ont été proposées ces dernières décennies pour les systèmes hyperboliques de lois de conservation [1,6,8,9] (et références incluses). Un haut degré de précision requérant une charge de calculs accrue, il est important que ces méthodes soient extensibles en contexte « massivement parallèle ». L'approche que nous proposons dans cette Note pour résoudre les équations d'Euler multidimensionnelles repose sur la technique des directions alternées avec des séquences de balayages d'ordre élevé au-delà du classique *splitting* de Strang, et sur une souche de schémas 1D performants particulièrement adaptée aux processeurs massivement multi-cœurs *et/ou* à l'accélération GPGPU (General Purpose Graphics Processing Unit). Contrairement aux techniques de type Runge–Kutta qui nécessitent à chaque sous-cycle un appel coûteux à l'équation d'état et une phase de communication entre sous-domaines, l'intégration en temps se fait en une seule passe grâce à la procédure de Cauchy–Kovalewska. La discrétisation spatiale n'utilise que des *stencils centrés* sur grille cartésienne régulière. Directement applicable à des équations d'état arbitraires, la méthode se distingue

E-mail addresses: frederic.duboc@cea.fr (F. Duboc), cedric.enaux@cea.fr (C. Enaux), stephane.jaouen@cea.fr (S. Jaouen), jourdren@cea.fr (H. Jourdren), wolff@ocre.cea.fr (M. Wolff).

1631-073X/$ – see front matter
doi:10.1016/j.crma.2009.12.008

également des travaux sus-cités par le fait qu'elle repose sur une formulation de type Lagrange-projection comme dans [3], restant toutefois ici d'ordre élevé en régime non linéaire.

Les schémas Lagrange-projection 1D permettant d'intégrer (1) entre t^n et t^{n+1} sont décrits en Section 2. Le schéma (3) permet dans un premier temps de résoudre ces équations en coordonnées lagrangiennes (2). Il repose sur l'évaluation du flux numérique $F^*_{i+1/2}$ qui, après intégration du développement de Taylor en temps de $F(U)$, est défini par (4). Très proche du flux *GoHy* présenté dans [5], son calcul utilise la procédure de Cauchy–Kovalewska pour remplacer les dérivées en temps par des dérivées en espace, ces dernières étant calculées à l'ordre voulu de la manière suivante : les quantités conservatives sont d'abord évaluées ponctuellement au centre de chaque maille par (5), ce qui permet, sans perte d'ordre, d'en déduire les valeurs ponctuelles de toute autre variable. Les termes apparaissant dans le calcul de $F^*_{i+1/2}$ sont alors évalués par (6) et les coefficients de la Table 1. A l'issue de cette étape, les quantités conservatives Eulériennes sont connues en t^{n+1} sur le maillage déformé (7) grâce à (12). La seconde étape consiste alors à projeter ces grandeurs sur la grille initiale, suivant (10), où le flux exact de projection (9) est approché à l'ordre voulu par (11) et une méthode classique de reconstruction centrée.

Ces schémas sont étendus en 2D en Section 3 par la méthode des directions alternées (le cas 3D, non développé ici, suit les mêmes lignes). Opérant sur des moyennes 1D, un schéma 1D doit être « encapsulé » par une interpolation (14) et une reconstruction (15) transverse. La séquence de balayages directionnels doit aussi être d'ordre élevé. Au-delà de l'ordre 2 et du classique splitting de Strang, des séquences venant de travaux sur les opérateurs symplectiques pour les systèmes Hamiltoniens sont utilisées [4,7]. A notre connaissance, de telles séquences, présentées dans la Table 2, sont appliquées ici pour la première fois aux systèmes hyperboliques non linéaires.

Les résultats numériques présentés en Section 4 sur l'advection d'un vortex 2D montrent que la précision théorique – ordre 2 à 6 – est atteinte. Pour les écoulements avec discontinuités, des techniques classiques non présentées dans cette Note (limiteurs, viscosités artificielles, etc.) peuvent alors être utilisées. La méthode retenue ici est celle décrite dans [2]. Contrairement aux techniques de limitation qui généralement « cassent » l'ordre de convergence [5], celle-ci présente l'avantage de conserver l'ordre théorique des schémas dans les zones régulières (Fig. 1a) tout en contrôlant l'amplitude des oscillations au voisinage des discontinuités (Fig. 1b). Ces résultats montrent que, bien qu'uniquement basée sur des discrétisations centrées, l'approche Lagrange-projection confère à ces schémas une bonne dissipation intrinsèque, rendant cette nouvelle souche de schémas éligible aux modèles de LES compressible.

1. Introduction

In recent decades, many high-order and/or high-resolution numerical methods have been proposed for hyperbolic systems of conservation laws [1,6,8,9] (and references therein). To take advantage of modern computers' architecture, such as many-core CPUs and/or General Purpose Graphics Processing Unit (GPGPU) acceleration, the finite volume schemes we propose in this Note for solving the nD Euler equations are based on efficient 1D schemes, which lie on centered discretizations on regular Cartesian grids without any Runge–Kutta sub-cycling, associated to a high-order dimensionally split method. Applicable to arbitrary equations of state (EOS), they also depart from the above mentioned works since they are based on a 1D Lagrange-remap formulation as in [3], but here the schemes are also high-order accurate in the nonlinear regime. Section 2 is devoted to the 1D case, Section 3 to its 2D extension (the 3D case follows the same lines) and Section 4 to numerical results.

In the following, k will denote the order of the scheme, $\overline{\phi}_i^n$ and ϕ_i^n will respectively denote the space averaged value of ϕ in the ith cell and its point-value in x_i at time t^n:

$$\overline{\phi}_i^n = \frac{1}{\Delta x_i} \int_{x_{i-\frac{1}{2}}}^{x_{i+\frac{1}{2}}} \phi\big(x, t^n\big)\,\mathrm{d}x \quad \text{and} \quad \phi_i^n = \phi\big(x_i, t^n\big).$$

2. High-order Lagrange-remap 1D schemes

We first consider the 1D hydrodynamics system (1) closed with an arbitrary EOS $p = p(\tau, S)$ where $\rho = 1/\tau$, u, p, e and S denote respectively the mass density, the velocity, the pressure, the specific total energy and entropy. Let ρ_0 be the initial mass density. Introducing the $(x,t) \to (X,t)$ variable change such that $\rho\,dx = \rho_0\,dX$, (1) rewrites (2) in Lagrangian coordinates. The Lagrange-remap method consists in the following two steps for integrating (1) between t^n and t^{n+1}. Let $\rho_0(x) = \rho(x, t^n)$, *i.e.* the regular Eulerian and Lagrangian grids $x_{i-\frac{1}{2}}$ and $X_{i-\frac{1}{2}}$ coincide at time t^n. First system (2) is time-integrated to give the Lagrangian conservative variables at time t^{n+1} on a non-uniform grid. These variables are then conservatively remapped on the initial grid, leading to the Eulerian conservative variables at time t^{n+1}.

$$\begin{cases} \partial_t \rho + \partial_x(\rho u) = 0, \\ \partial_t(\rho u) + \partial_x(\rho u^2 + p) = 0, \\ \partial_t(\rho e) + \partial_x(\rho e u + p u) = 0. \end{cases} \tag{1}$$

Table 1
Coefficients c_l^r, $\tilde{c}_l^r$ and $d_{m,l}^s$ with $r = \lfloor k/2 \rfloor$ and $s = \lceil k/2 \rceil$.

Tableau 1
Coefficients c_l^r, $\tilde{c}_l^r$ et $d_{m,l}^s$ avec $r = \lfloor k/2 \rfloor$ et $s = \lceil k/2 \rceil$.

	c_0^r	c_1^r	c_2^r	c_3^r	$\tilde{c}_0^r$	$\tilde{c}_1^r$	$\tilde{c}_2^r$	$\tilde{c}_3^r$
$r=1$	$\frac{13}{12}$	$-\frac{1}{24}$			$\frac{11}{12}$	$\frac{1}{24}$		
$r=2$	$\frac{1067}{960}$	$-\frac{29}{480}$	$\frac{3}{640}$		$\frac{863}{960}$	$\frac{77}{1440}$	$-\frac{17}{5760}$	
$r=3$	$\frac{30251}{26880}$	$-\frac{7621}{107520}$	$\frac{159}{17920}$	$-\frac{5}{7168}$	$\frac{215641}{241920}$	$\frac{6361}{107520}$	$-\frac{281}{53760}$	$\frac{367}{967680}$

	$d_{0,l}^1$	$d_{1,l}^1$	$d_{0,l}^2$	$d_{1,l}^2$	$d_{2,l}^2$	$d_{3,l}^2$	$d_{0,l}^3$	$d_{1,l}^3$	$d_{2,l}^3$	$d_{3,l}^3$	$d_{4,l}^3$	$d_{5,l}^3$
$l=1$	$\frac{1}{2}$	1	$\frac{9}{16}$	$\frac{9}{8}$	$-\frac{1}{2}$	-3	$\frac{75}{128}$	$\frac{75}{64}$	$-\frac{17}{24}$	$-\frac{17}{4}$	1	10
$l=2$			$-\frac{1}{16}$	$-\frac{1}{24}$	$\frac{1}{2}$	1	$-\frac{25}{256}$	$-\frac{25}{384}$	$\frac{13}{16}$	$\frac{13}{8}$	$-\frac{3}{2}$	-5
$l=3$							$\frac{3}{256}$	$\frac{3}{640}$	$-\frac{5}{48}$	$-\frac{1}{8}$	$\frac{1}{2}$	1

$$\begin{cases} \partial_t(\rho_0\tau) - \partial_X u = 0, \\ \partial_t(\rho_0 u) + \partial_X p = 0, \\ \partial_t(\rho_0 e) + \partial_X(pu) = 0, \end{cases} \tag{2}$$

2.1. Lagrangian step

Let $U = (\rho_0\tau, \rho_0 u, \rho_0 e)^t$ and $F(U) = (-u, p, pu)^t$. Integrating (2) over $[X_{i-\frac{1}{2}}; X_{i+\frac{1}{2}}] \times [t^n; t^{n+1}]$ and dividing the result by $(\Delta t \Delta X)$ leads to the following *exact* conservative formulation in Lagrangian coordinates:

$$\frac{\overline{U}_i^{n+1} - \overline{U}_i^n}{\Delta t} + \frac{F^*_{i+\frac{1}{2}} - F^*_{i-\frac{1}{2}}}{\Delta X} = 0 \quad \text{where } F^*_{i+\frac{1}{2}} = \frac{1}{\Delta t} \int_{t^n}^{t^{n+1}} F(U)(X_{i+\frac{1}{2}}, \theta)\, \mathrm{d}\theta. \tag{3}$$

After a Taylor expansion of the integrand, the numerical flux reads

$$F^*_{i+\frac{1}{2}} = \sum_{j=0}^{k-1} \frac{\Delta t^j}{(j+1)!} \cdot \frac{\partial^j F(U)}{\partial t^j}\big(X_{i+\frac{1}{2}}, t^n\big) + \mathcal{O}\big(\Delta t^k\big). \tag{4}$$

Temporal derivatives in (4) are replaced by spatial ones using the Cauchy–Kovalevskaya procedure[1] (see the very close *GoHy* fluxes in [5] for more details). To approximate $F(U)$ and the resulting spatial derivatives at cell boundaries, we first compute kth-order point-values of U using centered stencils:

$$U_i^n = U\big(X_i, t^n\big) + \mathcal{O}\big(\Delta X^k\big) = c_0^r \cdot \overline{U}_i^n + \sum_{l=1}^{r} c_l^r \cdot \big(\overline{U}_{i+l}^n + \overline{U}_{i-l}^n\big), \tag{5}$$

where $r = \lfloor k/2 \rfloor$ and c_l^r are defined in Table 1. This allows us to compute point-values of any non-conservative variable ψ_i^n without loss of accuracy. Each serie's term is then evaluated at the appropriate order of accuracy using centered formula (6), with $s = \lceil k/2 \rceil$ and $d_{m,l}^s$ defined in Table 1:

$$\left(\frac{\partial^m \psi}{\partial x^m}\right)^n_{i+\frac{1}{2}} = \left(\frac{\partial^m \psi}{\partial x^m}\right)\big(X_{i+\frac{1}{2}}, t^n\big) + \mathcal{O}\big(\Delta X^{k-m}\big) = \begin{cases} \frac{1}{\Delta x^m} \sum_{l=1}^{s} d_{m,l}^s \cdot (\psi_{i+l}^n + \psi_{i-l+1}^n) & \text{if } m \text{ is even,} \\ \frac{1}{\Delta x^m} \sum_{l=1}^{s} d_{m,l}^s \cdot (\psi_{i+l}^n - \psi_{i-l+1}^n) & \text{if } m \text{ is odd.} \end{cases} \tag{6}$$

Eulerian coordinates x, which evolve according to $\partial_t x(X,t) = u$, are also time-integrated:

$$x_{i+\frac{1}{2}}^{n+1} - x_{i+\frac{1}{2}} = \int_{t^n}^{t^{n+1}} u(X_{i+\frac{1}{2}}, \theta)\, \mathrm{d}\theta = u^*_{i+\frac{1}{2}} \Delta t. \tag{7}$$

Since u^* is computed at the desired order, either are the positions $x_{i+\frac{1}{2}}^{n+1}$ of the moving boundaries at t^{n+1}.

[1] Contrarily to Runge–Kutta methods, high-order accuracy is achieved in a single time step, requiring only one EOS call but more data from the states' surface (*i.e.* higher-order derivatives). With only one communication phase per 1D sweep and more computations per cell, these properties are ideal for domain decomposition methods and GPGPU acceleration.

2.2. Remapping step

After the Lagrangian step, conservative variables $(\rho\phi)$ for $\phi \in \{1, u, e\}$ are remapped on the initial regular grid $\{x_{i+\frac{1}{2}}\}$ according to the following integral splitting

$$\overline{(\rho\phi)}_i^{n+1} \overset{\text{def}}{=} \frac{1}{\Delta x}\int_{x_{i-\frac{1}{2}}}^{x_{i+\frac{1}{2}}} (\rho\phi)\big(x, t^{n+1}\big)\,\mathrm{d}x = \frac{1}{\Delta x}\int_{x_{i-\frac{1}{2}}}^{x_{i+\frac{1}{2}}^{n+1}} (\rho\phi) + \underbrace{\frac{1}{\Delta x}\int_{x_{i-\frac{1}{2}}^{n+1}}^{x_{i+\frac{1}{2}}^{n+1}} (\rho\phi)}_{(\mathcal{I})} + \frac{1}{\Delta x}\int_{x_{i+\frac{1}{2}}^{n+1}}^{x_{i+\frac{1}{2}}} (\rho\phi). \tag{8}$$

Using the $(x,t) \to (X,t)$ variable change in $(\mathcal{I})$ and introducing the *exact* remapping flux defined by

$$(\rho\phi)^*_{i+\frac{1}{2}} \overset{\text{def}}{=} \frac{1}{x^{n+1}_{i+\frac{1}{2}} - x_{i+\frac{1}{2}}}\int_{x_{i+\frac{1}{2}}}^{x_{i+\frac{1}{2}}^{n+1}} (\rho\phi)\big(x, t^{n+1}\big)\,\mathrm{d}x, \tag{9}$$

the remapping step reads, using (7):

$$\overline{(\rho\phi)}_i^{n+1} = \overline{(\rho_0\phi)}_i^{n+1} - \frac{\Delta t}{\Delta x}\big[u^*_{i+\frac{1}{2}}(\rho\phi)^*_{i+\frac{1}{2}} - u^*_{i-\frac{1}{2}}(\rho\phi)^*_{i-\frac{1}{2}}\big]. \tag{10}$$

It remains to compute (9) at the desired order. This is done by building an upwind kth-order polynomial reconstruction p^ϕ of $(\rho\phi)$ on the non-uniform grid $\{x^{n+1}_{i+\frac{1}{2}}\}$:

$$(\rho\phi)^*_{i+\frac{1}{2}} = \frac{1}{x^{n+1}_{i+\frac{1}{2}} - x_{i+\frac{1}{2}}}\int_{x_{i+\frac{1}{2}}}^{x_{i+\frac{1}{2}}^{n+1}} p^\phi_{up}(x)\,\mathrm{d}x \quad \text{where } up = i \text{ if } u^*_{i+\frac{1}{2}}\Delta t \geqslant 0 \text{ and } up = i+1 \text{ otherwise.} \tag{11}$$

Determining p^ϕ_i supposes to know the cell averages of $(\rho\phi)$ on the non-uniform grid $\{x^{n+1}_{i+\frac{1}{2}}\}$. This is achieved using the following *exact* formula

$$\frac{1}{\Delta x^{n+1}_i}\int_{x^{n+1}_{i-\frac{1}{2}}}^{x^{n+1}_{i+\frac{1}{2}}} (\rho\phi)\big(x, t^{n+1}\big)\,\mathrm{d}x = \frac{\overline{(\rho_0\phi)}^{n+1}_i}{\overline{(\rho_0\tau)}^{n+1}_i}. \tag{12}$$

These cell averages being evaluated, p^ϕ is computed using a classical 1D polynomial reconstruction on centered stencils (see [8] for example) and (11) is estimated either analytically or using appropriate Gauss quadrature formulae.

3. High-order multidimensional extension

Such 1D schemes are used with a dimensional splitting method (DSM) on the 2D Euler system:

$$\begin{cases} \partial_t\rho + \nabla.(\rho\boldsymbol{u}) = 0, \\ \partial_t(\rho\boldsymbol{\Phi}) + \nabla.(\rho\boldsymbol{\Phi}\otimes\boldsymbol{u} + \boldsymbol{f}) = 0, \end{cases} \quad \text{with } \boldsymbol{u} = \begin{pmatrix} u \\ v \end{pmatrix},\ \boldsymbol{\Phi} = \begin{pmatrix} \boldsymbol{u} \\ e \end{pmatrix} \text{ and } \boldsymbol{f} = \begin{pmatrix} pI_2 \\ p\boldsymbol{u}^t \end{pmatrix}. \tag{13}$$

The 1D scheme extension for the transverse impulsion equation is straightforward since $\partial_t(\rho_0 v) = 0$ in Lagrangian coordinates: one just has to apply the remapping step with $\phi = v$ and $\overline{(\rho_0 v)}^{n+1}_i = \overline{(\rho_0 v)}^n_i$. Two key points are however necessary in order to preserve high-order accuracy in 2D.

Since 1D schemes operate on 1D cell averages, they must be encapsulated by transverse interpolation and reconstruction. As an example, a x-dimensional sweep from t^n to t^{n+1} therefore consists in

1. Conservative centered y-interpolation, with c^r_l defined in Table 1:

$$\widehat{(\rho\phi)}^n_{i,j} = \frac{1}{\Delta x}\int_{x_{i-\frac{1}{2}}}^{x_{i+\frac{1}{2}}} (\rho\phi)\big(x, y_j, t^n\big)\,\mathrm{d}x + \mathcal{O}\big(\Delta y^k\big) = c^k_0\cdot\overline{(\rho\phi)}^n_{i,j} + \sum_{l=1}^{r} c^r_l\cdot\big(\overline{(\rho\phi)}^n_{i,j+l} + \overline{(\rho\phi)}^n_{i,j-l}\big), \tag{14}$$

Table 2
Weights w_i for the dimensional splitting method (DSM).

Tableau 2
Poids w_i pour le splitting directionnel.

	x	y	x	y	x	y
2nd-order DSM	0.50000000	1.00000000	0.50000000			
3rd-order DSM	0.26833009	0.91966152	−0.18799161	−0.18799161	0.91966152	0.26833009
4th-order DSM	0.50000000	−0.05032120	−0.27516060	0.55032120	0.55032120	0.55032120
	−0.27516060	−0.05032120	0.50000000			
5th- and 6th-order DSM	0.39225680	0.78451361	0.51004341	0.23557321	−0.47105338	−1.17767998
	0.06875316	1.31518632	0.06875316	−1.17767998	−0.47105338	0.23557321
	0.51004341	0.78451361	0.39225680			

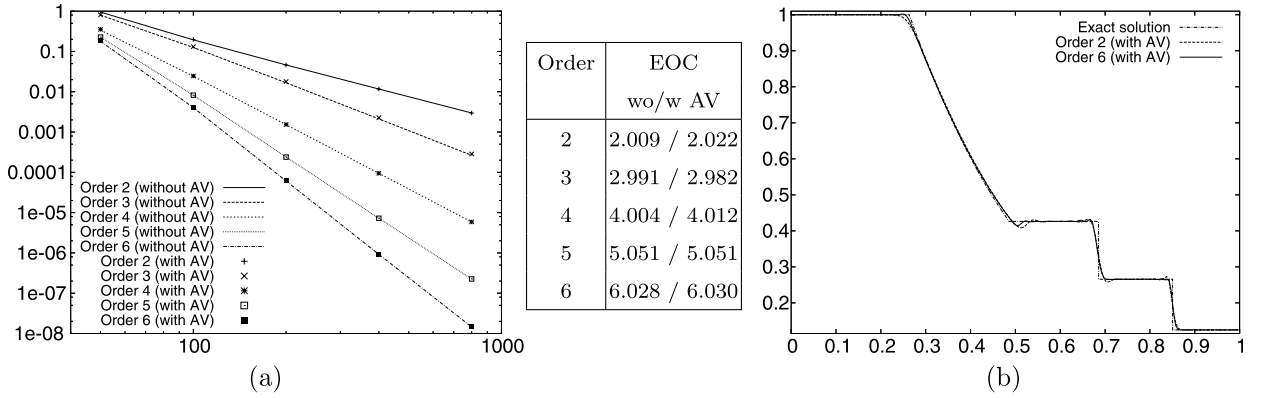

Fig. 1. (a) 2D vortex: L^1-error *vs* the number of cells per direction and EOC. (b) 1D Sod's shock tube on 200 cells.

2. 1D Lagrange-remap scheme which returns $\widehat{(\rho\phi)}_{i,j}^{n+1}$ on each grid line j.
3. Conservative centered y-reconstruction, with $\tilde{c}_l^r$ defined in Table 1:

$$\overline{(\rho\phi)}_{i,j}^{n+1} = \tilde{c}_0^r \cdot \widehat{(\rho\phi)}_{i,j}^{n+1} + \sum_{l=1}^{r} \tilde{c}_l^r \cdot \left(\widehat{(\rho\phi)}_{i,j+l}^{n+1} + \widehat{(\rho\phi)}_{i,j-l}^{n+1}\right). \tag{15}$$

High-order splitting sequences beyond the well-known 2nd-order Strang DSM (see Table 2) must also be used. Such sequences, which necessarily contain *negative* time steps, have been proposed in the case of symplectic integrators for Hamiltonian systems [4,7]. All above computations being centered, these can be used here without any particular treatment for handling such an *unusual* case. The kth-order DSM consists in alternatively applying the previous algorithm in the x- and y-direction with appropriate weighted-time increments $w_i \Delta t$. These weights are given in Table 2 and 3D sequences can be built recursively.

4. Numerical results

The experimental order of convergence (EOC) of the above schemes is measured on a 2D vortex advection test problem. The initial condition is given by (16), where $r^2 = x^2 + y^2$. Computations are performed on a $[-10:10]^2$ domain till $t = 1$ with $\rho_0 = p_0 = 1$, $\boldsymbol{u}_\infty = (1,1)^t$, $\gamma = 1.4$ and $\beta = 5$. The L^1-error in both space and time on $U = (\rho, \rho\boldsymbol{\Phi}^t)^t$ is reported in Fig. 1(a): the theoretical order is reached.

$$\rho(x,y) = \left(\rho_0 - \frac{(\gamma-1)\beta^2}{8\gamma\pi^2} e^{1-r^2}\right)^{\frac{1}{\gamma-1}}, \qquad p(x,y) = p_0\left(\frac{\rho(x,y)}{\rho_0}\right)^{\gamma},$$
$$\boldsymbol{u}(x,y) = \boldsymbol{u}_\infty + \frac{\beta}{2\pi} e^{\frac{1-r^2}{2}} (-y,x)^t. \tag{16}$$

For discontinuous flows, classical limiter techniques, which generally break the schemes' accuracy [5], or extra dissipation terms can be added. We have used here the artificial viscosity (AV) method proposed in [2].[2] Its advantage over limiter techniques is that it preserves the order of accuracy in smooth regions of the flow (Fig. 1a) while still damping the

[2] We have used relations (16)-(17) of [2] with $r = 2\lceil k/2 \rceil$ and $(C_\beta, C_\kappa) = (10,2)$, $(3,2)$ and $(1,0.5)$ for $r = 2$, 4 and 6 respectively.

oscillations near discontinuities (Fig. 1b). With only centered discretizations, these results show the quite good dissipative properties of the Lagrange-remap approach, making by the way these high-order schemes eligible to large-eddy simulation (LES) of compressible flows such as shock/turbulence interactions.

5. Conclusions

We have proposed a new class of high-order finite volume dimensionally split schemes for solving the nonlinear Euler equations. To our knowledge, high-order directional sequences are used here for the first time on nonlinear hyperbolic equations. Each directional sweep relies on efficient 1D Lagrange-remap schemes particularly well-suited for High Performance Computing parallelism (domain decomposition, many-core CPUs and/or GPGPU acceleration). The schemes operate on a regular Cartesian grid using exclusively centered stencils and time integration is achieved in a single step. Together with the artificial viscosity method of [2] we infer that this class of schemes is eligible to LES of compressible flows.

Ongoing work concerns multi-physics extensions of this class of schemes, most notably nT-hydrodynamics, elasticity and ideal magnetohydrodynamics.

References

[1] B. Cockburn, C.W. Shu, The Runge–Kutta discontinuous Galerkin method for conservation laws. V – Multidimensional systems, J. Comput. Phys. 141 (1998) 199–224.
[2] A.W. Cook, Artificial fluid properties for large-eddy simulation of compressible turbulent mixing, Phys. Fluids 19 (055103) (2007) 1–9.
[3] S. Del Pino, H. Jourdren, Arbitrary high-order schemes for the linear advection and wave equations: Application to hydrodynamics and aeroacoustics, C. R. Acad. Sci. Paris 342 (2006) 441–446.
[4] E. Forest, R.D. Ruth, Fourth-order symplectic integration, Physica D 43 (1990) 105–117.
[5] O. Heuzé, S. Jaouen, H. Jourdren, Dissipative issue of high-order shock capturing schemes with non-convex equation of state, J. Comput. Phys. 228 (2009) 833–860.
[6] G.S. Jiang, E. Tadmor, Nonoscillatory central schemes for multidimensional hyperbolic conservation laws, SIAM J. Sci. Comput. 19 (6) (1998) 1892–1917.
[7] R.I. McLachlan, P. Atela, The accuracy of symplectic integrators, Nonlinearity 5 (1992) 541–562.
[8] C.W. Shu, Essentially non-oscillatory and weighted essentially non-oscillatory schemes for hyperbolic conservation laws, in: Advanced Numerical Approximation of Nonlinear Hyperbolic Equations, Springer, 1998, pp. 325–432.
[9] E.F. Toro, V.A. Titarev, ADER schemes for three-dimensional non-linear hyperbolic systems, J. Comput. Phys. 204 (2005) 715–736.